数理解析研究所講究録
第1847巻 2013年 54-63

非ニュートン粘性複合ジェットの崩壊とカプセル形成領域

吉永隆夫*, 松本和樹
大阪大学 (Osaka Univ.)
yoshinag@me.es.osaka-u.ac.jp

1 Introduction

A gas or liquid-cored annular jet is called a compound liquid jet and of great importance in various engineering and industrial applications such as encapsulation techniques in foods, drugs and ink-jet printing systems [1, 2]. Breakup and encapsulation phenomena of the jet have been investigated experimentally and theoretically. Kendall [3] observed for a gas-cored jet that a train of liquid shells is naturally produced and their formation frequencies depend upon velocity ratios of the core to the annular phases. For a liquid-cored jet, Hertz and Hermanrud [4] observed two different types of encapsulation depending upon the surface tension of the interface between the core and annular phases.

On the other hand, using simplified nonlinear equations reduced by a long wave approximation, Yoshinaga and Maeda [5] analytically examined the breakup behavior of an inviscid jet. Yoshinaga [6] also showed that natural shell formation frequencies observed in the experiment for the gas-cored jet [3] are well predicted by using the most unstable frequencies of input disturbances which make the breakup time minimum. Later, Yoshinaga and Yamamoto [7] examined the viscous effects on the breakup of the jet. They found that the core phase is choked due to the viscous effect at the pinching and followed by the ballooning of the annular phase in the upstream. Although these results were obtained for small Reynolds numbers, the viscosity is assumed to be Newtonian. However, in order to understand production of the capsules in the practical use of the liquids like polymer solutions, it becomes important to examine the non-Newtonian effects on the breakup behavior. Then, since the viscosity departs from the Newtonian when the deformation rate becomes large, it is expected the the non-Newtonian effects appear for large deformation of the jet near the breakup.

In this paper, considering the non-Newtonian viscosity described by the Carreau model [8], a set of reduced nonlinear jet equations is analytically derived by means of a long wave approximation. The breakup behavior and encapsulation regime are numerically examined by using these equations for a semi-infinite jet when sinusoidal disturbances are applied at a nozzle exit of the jet.

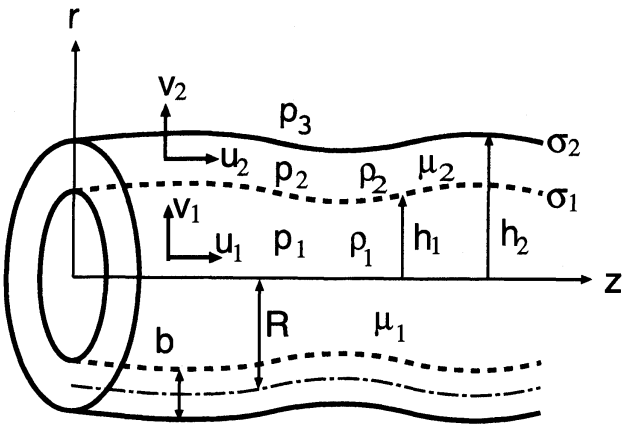

Figure 1: Schematic of a viscous compound liquid jet.

2 Formulation

Figure 1 shows the schematic of the jet in the (z, r) axisymmetric coordinate system. Noting that the subscript $j = 1$ is refereed to as the core phase or the inner interface and $j = 2$ as the annular phase or the outer interface, the velocity vectors are denoted by $\boldsymbol{u}_j$ whose components are (u_j, v_j), while the densities by ρ_j, the viscosities by μ_j, the surface tensions of the interfaces by σ_j and the pressures by p_j. The surfaces are specified at $r = h_j$, while the pressure of the surrounding ambient gas p_3 is constant and the density is ignored. For convenience of the later analysis, the thickness of the annular phase b $(= h_2 - h_1)$ and the radius of the mid-plane of the annular phase R $(= (h_2 + h_1)/2)$ are introduced.

In the analysis, we assume that the core and annular phases are incompressible and the gravitational force is ignored. The basic equations are then given by the continuity and momentum equations for the core phase $(j = 1,\ 0 \le r < h_1)$ and the annular phase $(j = 2,\ h_1 < r < h_2)$ as follows:

$$\frac{\partial u_j}{\partial z} + \frac{1}{r}\frac{\partial (r v_j)}{\partial r} = 0, \tag{1}$$

$$\rho_j\Big(\frac{\partial u_j}{\partial t} + u_j\frac{\partial u_j}{\partial z} + v_j\frac{\partial u_j}{\partial r}\Big) = -\frac{\partial p_j}{\partial z} + \frac{1}{r}\frac{\partial}{\partial r}\Big[\mu_j r\Big(\frac{\partial v_j}{\partial z} + \frac{\partial u_j}{\partial r}\Big)\Big] + \frac{\partial}{\partial z}\Big(2\mu_j\frac{\partial u_j}{\partial z}\Big), \tag{2}$$

$$\rho_j\Big(\frac{\partial v_j}{\partial t} + u_j\frac{\partial v_j}{\partial z} + v_j\frac{\partial v_j}{\partial r}\Big) = -\frac{\partial p_j}{\partial r} + \frac{1}{r}\frac{\partial}{\partial r}\Big(2\mu_j r\frac{\partial v_j}{\partial r}\Big) + \frac{\partial}{\partial z}\Big[\mu_j\Big(\frac{\partial v_j}{\partial z} + \frac{\partial u_j}{\partial r}\Big)\Big] - 2\mu_j\frac{v_j}{r^2}. \tag{3}$$

On the other hand, the boundary conditions are given as the kinematical conditions

$$\frac{\partial h_1}{\partial t} = v_1 - u_1\frac{\partial h_1}{\partial z} = v_2 - u_2\frac{\partial h_1}{\partial z}, \quad \boldsymbol{u}_1 = \boldsymbol{u}_2 \text{ on } r = h_1, \tag{4a}$$

$$\frac{\partial h_2}{\partial t} = v_2 - u_2\frac{\partial h_2}{\partial z} \text{ on } r = h_2, \tag{4b}$$

and the dynamical conditions

$$p_1 = p_2 + (\boldsymbol{D}_1\boldsymbol{n}_1)\cdot\boldsymbol{n}_1 - (\boldsymbol{D}_2\boldsymbol{n}_1)\cdot\boldsymbol{n}_1 + \sigma_1\kappa_1 \text{ and } (\boldsymbol{D}_1\boldsymbol{n}_1)\cdot\boldsymbol{t}_1 = (\boldsymbol{D}_2\boldsymbol{n}_1)\cdot\boldsymbol{t}_1 \quad \text{on } r = h_1, \tag{5a}$$

$$p_2 = p_3 + (\boldsymbol{D}_2\boldsymbol{n}_2)\cdot\boldsymbol{n}_2 + \sigma_2\kappa_2 \text{ and } (\boldsymbol{D}_2\boldsymbol{n}_2)\cdot\boldsymbol{t}_2 = 0 \quad \text{on } r = h_2. \tag{5b}$$

In the above representations,

$$\boldsymbol{n}_j = \frac{(-\partial h_j/\partial z, 1)}{[1+(\partial h_j/\partial z)^2]^{1/2}} \quad \text{and} \quad \boldsymbol{t}_j = \frac{(1, \partial h_j/\partial z)}{[1+(\partial h_j/\partial z)^2]^{1/2}},$$

are, respectively, the normal and tangential vectors and

$$\boldsymbol{D}_j = \mu_j \begin{bmatrix} 2\partial u_j/\partial z & (\partial v_j/\partial z + \partial u_j/\partial r) \\ (\partial v_j/\partial z + \partial u_j/\partial r) & 2\partial v_j/\partial r \end{bmatrix},$$

are the viscous stress tensors, while the surface tensions $\sigma_1\kappa_1$ and $\sigma_2\kappa_2$ act on the surfaces when the curvatures are given as

$$\kappa_j = \frac{1}{h_j\left[1+(\partial h_j/\partial z)^2\right]^{1/2}} - \frac{\partial^2 h_j/\partial z^2}{\left[1+(\partial h_j/\partial z)^2\right]^{3/2}}.$$

The non-Newtonian viscosity is presented by the following Carreau model [8]:

$$\mu_j = \mu_{0j} M_j \quad \text{and} \quad M_j = \left[1+(\alpha\dot{\gamma}_j)^2\right]^{(n-1)/2}, \tag{6}$$

where μ_j are the apparent viscosities and $\dot{\gamma}_j$ are the deformation rates which are given as the second invariant in terms of u_j and v_j in the following forms ($j = 1, 2$):

$$\dot{\gamma}_j = \sqrt{2\left(\frac{\partial v_j}{\partial r}\right)^2 + 2\left(\frac{v_j}{r}\right)^2 + \left(\frac{\partial v_j}{\partial z} + \frac{\partial u_j}{\partial r}\right)^2 + 2\left(\frac{\partial u_j}{\partial z}\right)^2}.$$

In the representations of (6), the time constant α takes about 1 to 10 depending upon materials, while the power low exponent n (> 0) takes less than 1 when the viscosity is pseudo-plastic and larger than 1 when dilatant and unity when Newtonian.

The basic equations and the boundary conditions can be simplified by using the long wave approximation in which sufficiently long waves are considered compared with the core radius and annular thickness. In the present analysis, we introduce the approximation with different expansion parameters to the core and the annular phases. Then, we assume the variables of the core phase to be expanded in terms of r^2 due to the axisymmetry at $r = 0$, while the annular phase in terms of $r - R$ as follows:

$$\begin{aligned} u_1 &= u_1^{(0)} + r^2 u_1^{(2)} + \cdots, \quad p_1 = p_1^{(0)} + r^2 p_1^{(2)} + \cdots, \\ u_2 &= u_2^{(0)} + (r-R)u_2^{(1)} + (r-R)^2 u_2^{(2)} + \cdots, \\ v_2 &= v_2^{(0)} + (r-R)v_2^{(1)} + (r-R)^2 v_2^{(2)} + \cdots, \\ p_2 &= p_2^{(0)} + (r-R)p_2^{(1)} + (r-R)^2 p_2^{(2)} + \cdots, \end{aligned} \tag{7}$$

where the coefficients are functions of z and t. The jet equations are derived in a similar way to the Newtonian viscous case [7]. Using the above expansions (7) into the basic equations and the boundary conditions (1)-(5) and the representations of the viscosity (6), and neglecting the higher order terms than $O(h_1)$ and $O(b)$, we finally obtain the following reduced equations for b, R, u_1, u_2, v_2 in the lowest order of the approximation (superscripts on the variables have been omitted):

$$\frac{\partial b}{\partial t} = -\frac{\partial (bu_2)}{\partial z} - \frac{bv_2}{R}, \tag{8a}$$

$$\frac{\partial R}{\partial t} = v_2 - u_2 \frac{\partial R}{\partial z}, \tag{8b}$$

$$\frac{\partial u_1}{\partial t} = -u_1 \frac{\partial u_1}{\partial z} - \frac{1}{\rho}\frac{\partial p_1}{\partial z} + \frac{\mu}{\rho \mathrm{Re}}\left(M_1 f_{11} + \frac{\partial M_1}{\partial z} f_{12}\right), \tag{8c}$$

$$\begin{aligned}\frac{\partial u_2}{\partial t} = &-u_2 \frac{\partial u_2}{\partial z} - \left(\frac{\partial P}{\partial z} - \frac{\Delta P}{b}\frac{\partial R}{\partial z}\right) + \frac{\mu}{\mathrm{Re}}\left(M_1 f_{21} + \frac{\partial M_1}{\partial r} f_{22}\right) \\ &+ \frac{1}{\mathrm{Re}}\left(M_2 f_{23} + \frac{\partial M_2}{\partial r} f_{24} + \frac{\partial M_2}{\partial z} f_{25}\right),\end{aligned} \tag{8d}$$

$$\frac{\partial v_2}{\partial t} = -u_2 \frac{\partial v_2}{\partial z} - \frac{\Delta P}{b} + \frac{\mu}{\mathrm{Re}} M_1 f_{31} + \frac{1}{\mathrm{Re}}\left(M_2 f_{32} + \frac{\partial M_2}{\partial r} f_{33} + \frac{\partial M_2}{\partial z} f_{34}\right), \tag{8e}$$

together with the equation for p_1 to connect the motions of the core and annular phases

$$A_1 \frac{\partial^2 p_1}{\partial z^2} + A_2 \frac{\partial p_1}{\partial z} + A_3 p_1 + A_4 = 0. \tag{8f}$$

In the above representations,

$$P = \tfrac{1}{2}(p_1 + p_3) - \tfrac{1}{2\mathrm{Wb}}(\sigma\kappa_1 - \kappa_2), \quad \Delta P = -(p_1 - p_3) + \frac{1}{\mathrm{Wb}}(\sigma\kappa_1 + \kappa_2),$$

are, respectively, like a mean pressure and a pressure difference of p_1 and p_3(=const.) when the surface tension is taken into account. The above set of equations have been normalized in terms of a characteristic length H, speed U, time H/U and pressure $\rho_2 U^2$, while the non-dimensional parameters of the Weber number $\mathrm{Wb} = \rho_2 H U^2/\sigma_2$, the Reynolds number $\mathrm{Re} = \rho H U/\mu_2$, the density ratio $\rho = \rho_1/\rho_2$, the viscosity ratio $\mu = \mu_{01}/\mu_{02}$ and the surface tension ratio $\sigma = \sigma_1/\sigma_2$ are introduced based on the annular phase. We can show that the viscous terms f_{ij} ($i = 1, 2, 3$, $j = 1, 2, \cdots$) in Eqs.(8c) to (8e) are functions of b, R, u_1, u_2, v_2, while the coefficients A_1 to A_4 in (8f) are functions of b, R, u_1, u_2, v_2 including f_{ij} and κ_j together with Re, μ, σ and ρ. Consequently, the problem can be reduced to solving the above simplified nonlinear equations (8a) to (8f).

In particular, for an infinitely long jet on the steady state without any velocity difference between the core and annular phases, we take the radii and flow velocities to be constant such as $h_1 = \bar{h}_1$, $h_2 = \bar{h}_2$, $u_1 = \bar{u}_1 = u_2 = \bar{u}_2$, $\bar{v}_1 = \bar{v}_2 = 0$. Then, we can set $f_{ij} = 0$ and $\Delta P = 0$, from which $\bar{p}_1$ is found to be always larger than p_3 due to the surface tension

$$\bar{p}_1 = p_3 + \frac{1}{\mathrm{Wb}}\left(\frac{\sigma}{\bar{R} - \bar{b}/2} + \frac{1}{\bar{R} + \bar{b}/2}\right), \tag{9}$$

where $\bar{R} = (\bar{h}_1 + \bar{h}_2)/2$, $\bar{b} = \bar{h}_2 - \bar{h}_1$.

Next we are going to numerically examine initial-boundary value problems for disturbances superimposed on the above steady state, where the characteristic values are chosen as $H = \bar{h}_2$ and $U = \bar{u}_2$.

3 Numerical Results

Numerical calculations are carried out by means of the 4th order Runge-Kutta method for the time derivatives and the finite difference method for the spatial derivatives, where the 3rd-order upwinding scheme is used for the convective terms and the central difference method whose error is of $O(\Delta z^2)$ is used for the other spatial derivatives. The numerical time and spatial grid sizes Δt and Δz are, respectively, taken to be 0.05 and 0.2 for most of the calculations, for which sufficient numerical accuracy is retained with respect to the volumes of the core and annular phases. We consider the initial-boundary value problems that the jet is in the steady state whose pressure difference is given by Eq.(9) for $0 \leq z < \infty$ when $t = 0$, while the velocity disturbances

$$u_1 - 1 = u_2 - 1 = \eta \sin(\omega t), \tag{10}$$

are applied to the nozzle exit at $z = 0$ for $t > 0$. In the calculations, the amplitude of disturbance η is taken to be 0.005 and the domain region of z for the calculations is taken to be enough large comparing with the breakup distance z_b (in most of the cases, z =200 to 300).

In the analysis, we examine the breakup time t_b and distance z_b for various input frequency ω, where we decide the breakup when the core radius or the annular thickness becomes sufficiently small to the extent of 0.001. Resulting from this, we can determine the critical frequencies ω_c which minimize t_b for each parameters Wb, Re, and σ. Such frequencies ω_c are the most unstable input frequencies in the sense of nonlinearity and can well predict the natural formation periods of capsules [6]. This is expected to be still valid in the preset case. In the following, unless noted otherwise, we take $\rho = 1$, $\mu = 1$, $\bar{u}_1 = \bar{u}_2 = 1$, $\bar{h}_1 = 0.485$ and $\bar{h}_2 = 1$ as the basic parameters according to the experiment for the liquid-cored jet by Hertz and Hermanrud [4]. All of the presented results are those at ω_c resulting from carrying out the calculations for various input ω from 0.2 to 1.6 for each parameters. In addition, we take $\alpha = 0.5$ and $n = 0.2$ and 1.8 for the non-Newtonian viscosities, while $n = 1$ for the Newtonian viscosity in Eq.(6).

First, we consider the weak viscous case of Re = 395 and Wb = 47.9 whose values are of the experiment [4]. Figure 2 for sufficiently small $\sigma = 0.1$ shows that the jet breaks up like a single phase column jet where the core phase pinches by closing the annular phase, which is expected to produce a train of liquid capsules. On the other hand, Fig.3 for larger $\sigma = 2.6$ shows that the core phase becomes unstable to be pinched prior to the annular phase because of larger surface tension ratio, which is expected to produce a train of core liquid drops in the sheath of annular phase and delay the the annular phase instability. We note that these breakup profiles are closely similar to the experimental results [4]. However, for different values of n , we cannot find any salient discrepancies not only in the breakup profiles, but also in the breakup time t_b and distance z_b and the

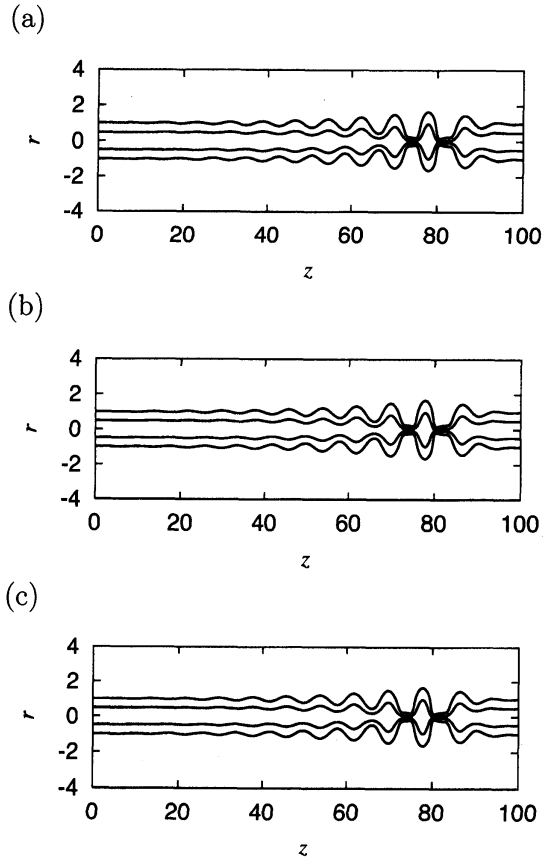

Figure 2: Breakup profiles for different n when $\sigma = 0.1$, Re = 354 and Wb = 47.9 ;(a)$n = 0.2$ ($t_b = 85.90$, $z_b = 80.60$, $\omega_c = 0.80$), (b)$n = 1$($t_b = 85.95$, $z_b = 80.60$, $\omega_c = 0.80$) and (c)$n = 1.8$ ($t_b = 85.95$, $z_b = 80.60$, $\omega_c = 0.78$).

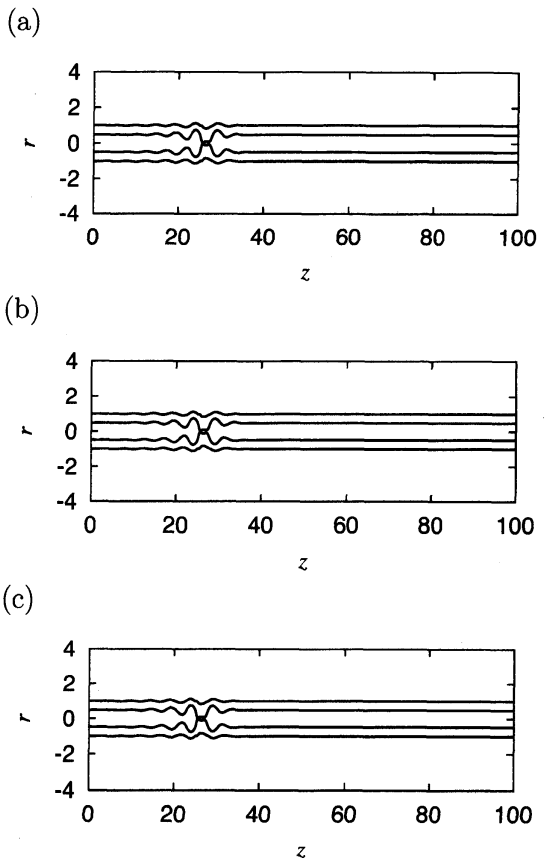

Figure 3: Breakup profiles for different n when $\sigma = 2.6$, Re = 354 and Wb = 47.9;(a)$n = 0.2$ ($t_b = 28.75$, $z_b = 25.80$, $\omega_c = 1.35$), (b)$n = 1$ ($t_b = 28.75$, $z_b = 25.80$, $\omega_c = 1.35$) and (c)$n = 1.8$ ($t_b = 28.80$, $z_b = 25.80$, $\omega_c = 1.35$).

critical frequency ω_c among (a), (b) and (c) in each Figs.2 and 3, where (a)$t_b = 85.90$, $z_b = 80.60$, $\omega_c = 0.80$, (b)$t_b = 85.95$, $z_b = 80.60$, $\omega_c = 0.80$ and (c)$t_b = 85.95$, $z_b = 80.60$ and $\omega_c = 0.78$ in Fig.2, while (a)$t_b = 28.75$, $z_b = 25.80$, $\omega_c = 1.35$, (b)$t_b = 28.75$, $z_b = 25.80$, $\omega_c = 1.35$ and (c)$t_b = 28.80$, $z_b = 25.80$, $\omega_c = 1.35$ in Fig.3. This shows that the non-Newtonian viscosity does not affect the breakup properties when the viscosity is weak or large Re.

Next we consider the more viscous case of Re = 10. Figure 4 for $\sigma = 0.1$ shows that the non-Newtonian viscosity does not still affect the breakup properties such as the breakup time and distance and critical frequency as well as the breakup profiles among (a), (b) and (c), where (a)$t_b = 211.15$, $z_b = 200.80$, $\omega_c = 0.50$, (b)$t_b = 205.50$, $z_b = 200.80$, $\omega_c = 0.50$ and (c)$t_b = 205.55$, $z_b = 200.80$ and $\omega_c = 0.50$. We note that t_b and z_b increase and ω_c decreases as the decrease of Re in comparison between Fig.2 and Fig.4. However, Fig.5 for $\sigma = 2.6$ and Wb = 80 shows that the profiles are significantly different for different

n. In the Figure, we find that the jet shows the typical three different breakups, that is, disintegration of the annular phase for $n = 0.2$ and the large ballooned annular phase when $n = 1$ and the closing of the annular phase with pinching the core phase when $n = 1.8$. In spite of the fact that the breakup profiles and ω_c are different for n, there is little discrepancy in the breakup time and distance, where (a)$t_b = 111.95$, $z_b = 109.40$, $\omega_c = 0.72$, (b)$t_b = 122.20$, $z_b = 120.00$, $\omega_c = 0.58$ and (c)$t_b = 125.80$, $z_b = 120.60$, $\omega_c = 0.40$. This means that the deformations of the jet are accelerated rapidly only near the breakup. As a result, the non-Newtonian viscosity may bring about these three types of breakup depending upon the values of n when Re is small and σ is not sufficiently small.

Since the breakup due to closing of the core phase is preferable for encapsulation and the disintegration or ballooning of the annular phase should be avoided for successful capsule producing, it is worth to reveal what types of the breakup tend to appear in the parameter region of Wb and σ. In Fig.6 we show the classification of the breakup profiles in the parameter regions for $n = 0.2$, 1 and 1.8 when Re = 10, where the symbols △, ○ and ● denote that the breakup is caused by the disintegration, ballooning and closing, respectively, corresponding to (a), (b) and (c) in Fig.5. We can find from Fig.6(a) for $n = 0.2$, the breakup is almost due to disintegration except for small σ. On the other hand, from Fig.6(b) for $n = 1$ the parameter region of closing increases and the region of disintegration is replaced by the ballooning, where the disintegration without ballooning is placed in between the closing and ballooning in most of the cases, though the breakup by the ballooning is finally caused by disintegration of the annular phase. However, we find in Fig.6(c) for n=1.8 that the region of the disintegration disappears and the region of closing more increases. These characteristic breakup profiles for different n show that the breakup is often caused by disintegration when the viscosity decreases as the increase of the deformation rate $\dot{\gamma}$ ($n < 1$), while the breakup is often by closing when the viscosity increases as the increase of $\dot{\gamma}$ ($n > 1$).

In spite of these three distinct breakup profiles for different n, we cannot find so evident discrepancies in the breakup time and distance. This is shown in Fig.7, where variations of ω_c, t_b and z_b are presented in (a), (b) and (c) when Wb and σ (= 1 and 4) are given, in each of which the cases of $n = 0.2$, 1 and 1.8 are, respectively, denoted by △, ○ and ●. It is found from the Figure that the values of t_b and z_b for different n agree well with each other unless Wb is so large, though ω_c are rather different for n. This means that the effects of the non-Newtonian viscosity appear only near the breakup since the breakup time and distance are little affected by n even if the breakup profiles are rather different.

Since most of the polymer liquids for the practical use are pseudo-plastic ($n < 1$), the jet is apt to break up by disintegration of the annular phase at the encapsulation for low Re. Therefore, we need to set suitable experimental condition and choose proper materials for successful capsule formation.

4 Conclusions

By using the long wave approximation we have derived the nonlinear equations of the non-Newtonian viscous compound liquid jet. Resulting from the numerical analysis for

the most unstable input frequencies when sinusoidal disturbances are fed at the nozzle exit of the semi-infinite jet, the following conclusions are obtained :

1. For larger Reynolds numbers Re, the jet breaks up like a single phase column jet when σ is sufficiently small, while the core phase breaks up by pinching before closing of the annular phase for larger σ. Any influence of the non-Newtonian viscosity on the breakup properties is not observed for different values of n.

2. For smaller Re, the jet still breaks up like a single phase column jet as long as σ is sufficiently small. The non-Newtonian viscosity also does not affect the breakup properties for different values of n.

3. When σ becomes large for small Re, however, the breakup profiles become different depending upon n in the non-Newtonian viscosity. For smaller n (< 1), the jet tends to break up by disintegration of the annular phase, while the breakup for larger n (> 1) mainly results from the ballooning or closing of the annular phase. Generally, as the increase of n, the breakup by closing of the annular phase is more dominant in the Wb and σ parameter region.

4. The influence of the non-Newtonian viscosity on t_b and z_b is not so large even when small Re and large σ. This means that the effect of non-Newtonian viscosity appears only near the breakup of the jet.

5. The jet using polymer liquids for small Re is apt to be subject to the annular phase disintegration, which prevents the successful encapsulation.

Acknowledgment

This work has been partially supported by the Grant-in-Aid for Science Research from the Ministry of Education, Culture, Sports, Science and Technology of Japan (No.21560177).

References

[1] Lefebvre,A.H., *Atomization and sprays* (Hemisphere, New York, 1989).

[2] Lin,S.P., *Breakup of liquid sheets and jets* (Cambridge, 2003).

[3] Kendall,J.M., *Phys. Fluids* 29, 2086-2094 (1986).

[4] Hertz, C.H. and Hermanrud, B., *J. Fluid Mech.* 131, 271 - 287 (1983).

[5] Yoshinaga,T. and Maeda,M., *J. Fluid Science and Technology* 4, 324-334 (2009).

[6] Yoshinaga,T.,*ICLASS 2009, Colorado, USA* July 26-30, 2009.

[7] Yoshinaga,T and Yamamoto,K., *J. Fluid Science and Technology* 6, 477-486 (2011).

[8] Carreau,P.J.,Kee,D.D. and Daroux,M., *Can.J.Chem.Eng.* 57, 135-140 (1979).

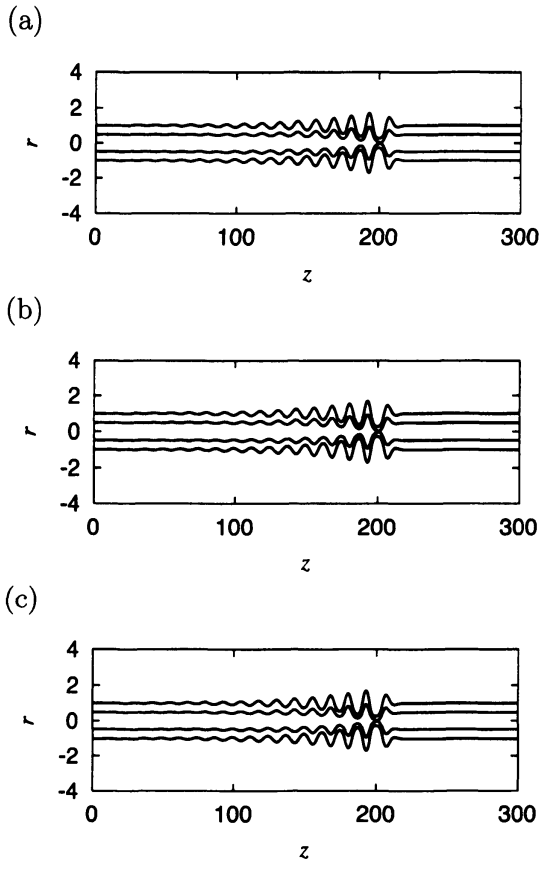

Figure 4: Breakup profiles for different n when $\sigma = 0.1$, Re $= 10$ and Wb $= 47.9$: (a)$n = 0.2$ ($t_b = 211.15$, $z_b = 200.80$, $\omega_c = 0.50$), (b)$n = 1$ ($t_b = 205.50$, $z_b = 200.80$, $\omega_c = 0.50$) and (c)$n = 1.8$ ($t_b = 205.55$, $z_b = 200.80$, $\omega_c = 0.50$).

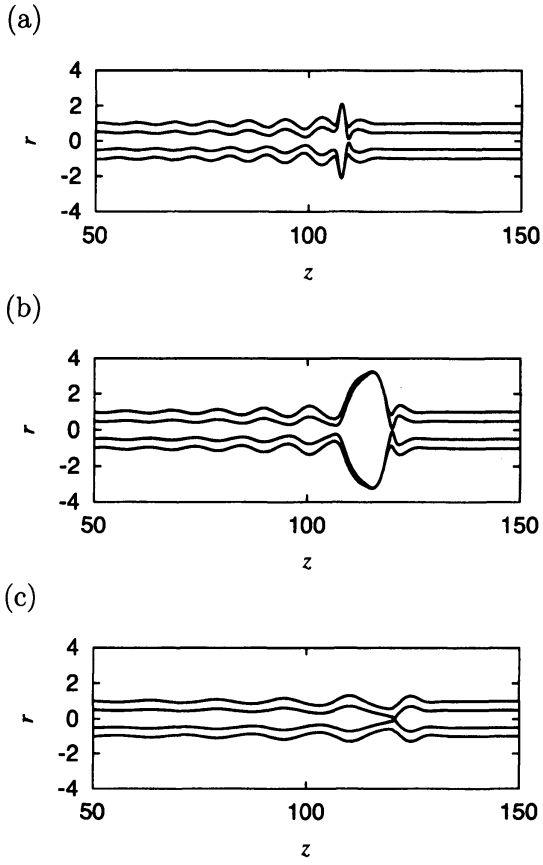

Figure 5: Typical three breakup profiles - disintegration, ballooning and closing- for different n when $\sigma = 2.6$, Re $= 10$ and Wb $= 80$; (a)$n = 0.2$ ($t_b = 111.95$, $z_b = 109.40$, $\omega_c = 0.72$), (b)$n = 1$ ($t_b = 122.20$, $z_b = 120.00$, $\omega_c = 0.58$) and (c)$n = 1.8$ ($t_b = 125.80$, $z_b = 120.60$, $\omega_c = 0.40$).

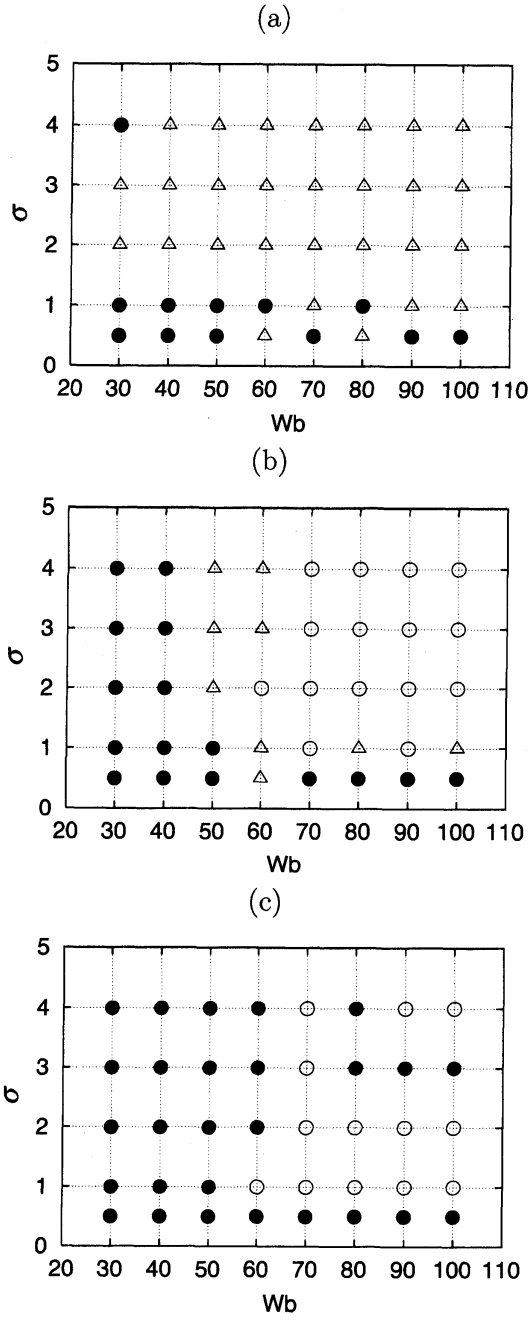

Figure 6: Classifications of the breakup profiles in the parameter space Wb and σ when Re = 10, where △, ○ and ●, respectively, denote the cases when the breakup is due to disintegration, ballooning and closing of the annular phase: (a)n = 0.2, (b)n = 1 and (c)n = 1.8.

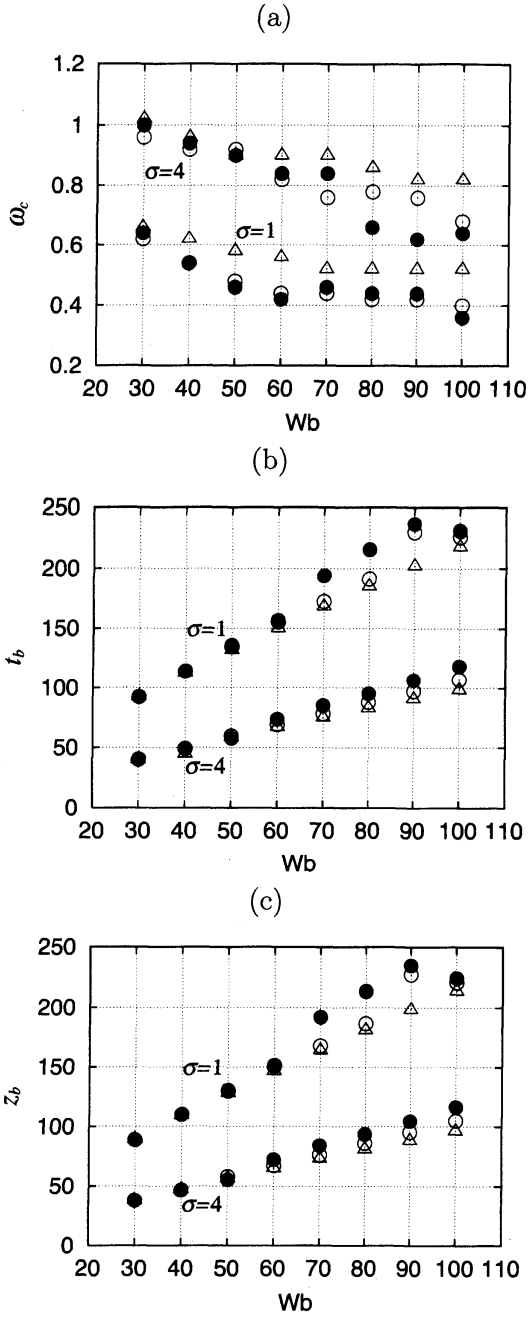

Figure 7: Variations of ω_c, t_b and z_b for Wb when σ = 1 and 4 and Re = 10, where △:n = 0.2, ○:n = 1 and ●:n = 1.8.